Supplementary Information

Mechanism-based corrector combination synergistically restores ΔF508-CFTR folding and function in cystic fibrosis

Tsukasa Okiyoneda[1,11], Guido Veit[1], Johanna F. Dekkers[2,3,4], Miklos Bagdany[1], Naoto Soya[1], Haijin Xu[1], Ariel Roldan[1], A. S. Verkman[5], Mark Kurth[6], Agnes Simon[7], Tamas Hegedus[8], Jeffrey M. Beekman[2,3,4], Gergely L. Lukacs[1,9,10]

[1]Department of Physiology, [9]Biochemistry and [10]GRASP, McGill University, Montréal, Quebec H3G 1Y6, Canada, [2]Department of Pediatric Pulmonology, [3]Department of Immunology, [4]Centre for Molecular and Cellular Intervention, University Medical Centre, Utrecht, The Netherlands, [5]Departments of Medicine and Physiology, University of California San Francisco, San Francisco, [6]Department of Chemistry, University of California Davis, Davis, California, [7]Department of Molecular Pharmacology, Research Center for Natural Sciences, Hungarian Academy of Sciences, Budapest, Hungary, [8]MTA-SE Molecular Biophysics Research Group and Department of Biophysics and Radiation Biology, Semmelweis University, Budapest, Hungary

Correspondence should be addressed to:
G. L. Lukacs
Department of Physiology, McGill University
3655 Promenade Sir-William-Osler, Montreal, Quebec H3G 1Y6, Canada
gergely.lukacs@mcgill.ca, Ph: 514-398-5582

[11]Current address: Department of Bioscience, School of Science and Technology, KwanseiGakuin University, Sanda, Hyogo 669-1337, Japan

Supplementary Results

Supplementary Figure Legends
Supplementary Figures 1 to 13
Supplementary Tables 1-3

Supplementary Figure 1. Schematic models of CFTR folding and ΔF508-induced misfolding.

(a) In the WT CFTR, MSD1 (M1), NBD1 (N1), MSD2 (M2) and NBD2 (N2) folds co-translationally to metastable states. Coupled domain folding and assembly facilitate proper domain-domain interaction and *vice versa*, and energetically favor the native tertiary structure formation of CFTR. Progressive enthalpic stabilization of individual domains during co- and post-translational folding is indicated by pseudo-colors. In case of the ΔF508 mutation, both NBD1 energetics and domain-domain interactions (primarily the NBD1-MSD1/2 interface) are impaired due to the conformational and topological defects, rendering all four major domains structurally unstable[6]. (b) Strategies to rescue the ΔF508-CFTR folding defect. While either stabilization of ΔF508-NBD1 or the NBD1-MSD2 interface by second site suppressor mutations such as 3S and R1S or R1070W and V510D, respectively, achieves modest improvement in the ΔF508-CFTR folding (<20%), simultaneous stabilization of these primary structural defects can lead to robust rescue (~80%)[26]. In analogy, available correctors may only restore one of the primary structural defects that may account for the limited rescue efficiency of ΔF508-CFTR. Corrector pairs acting on different primary structural defects, however, likely restore ΔF508-CFTR folding synergistically. Suppressor mutations can be instrumental for a structural based corrector screening to identify correctors that either stabilize the NBD1 and/or the NBD1-MSD2 interface based on the possible synergism.

Supplementary Figure 2. Differential correction efficiency of ΔF508 CFTR containing stabilized NBD1 or NBD1-MSD2 interface in BHK cells.

(a) PM density of ΔF508-CFTR containing R1S (left) or R1070W (right) mutations was measured by cell surface ELISA using anti-HA Ab and expressed as % of WT CFTR. BHK cells, stably expressing the indicated construct, were treated with correctors for 24 h at 37°C. These results were

also plotted in Fig.1b-c. Red and green bars indicate correctors that belong to class-I and class-II, respectively. Grey bars represent dual acting corrector-potentiator compounds. Data are means ± SEM (n=6-12). The augmented PM density of ΔF508-CFTR after corrector treatment in the presence of either R1S (Res_{R1S}) or R1070W (Res_{R1070W}) mutation is expressed as percentage of the WT PM level. (b-c) Second site suppressor mutations differentially enhance the ΔF508-CFTR rescue by class-I correctors. The PM density (b) and steady-state expression (c) of ΔF508-CFTR variants were determined by ELISA (means ± SEM, n=8) and Western blotting with anti-HA Ab, respectively. The PM density data were also plotted in Fig.1e (Y-axis). Na^+/K^+-ATPase (ATPase) was used as a loading control. Cells were treated with correctors (10 μM C3, 3 μM C18 or 3 μM VX809) for 24 h at 37°C. B, immature core-glycosylated; C, mature complex-glycosylated form. (d) The maturation efficiency of ΔF508-CFTR measured by metabolic pulse-chase experiments shown in Fig.1d was quantified by densitometry (mean ± SEM, n=3-4).

Supplementary Figure 3. Suppressor mutations and correctors efficiently rescue the PM expression and function of ΔF508-CFTR in polarized CFBE41o- epithelial cells.

(a-d) The consequence of suppressor mutations-induced NBD1 and/or NBD1-MSD2 interface stabilization on the PM density, complex-glycosylation and function of ΔF508-CFTR in CFBE41o- cells. The steady-state expression (a), PM density (b, n=12-24) and apical Cl^- current (c-d, n=3-4) of ΔF508-CFTR-3HA were measured by Western blotting, ELISA and short circuit current, respectively. Data represent means ± SEM. CFTR expression was induced for 3-4 days with doxycycline as described in Methods. (e) The effect of class-I corrector combination with suppressor mutations on the apical chloride current. Representative apical Cl^- currents obtained in polarized CFBE41o- cells expressing the indicated CFTR variants after 24 h pre-treatment with or

without correctors (3μM C18 or VX-809) at 37°C. The measurements were performed in presence of a basolateral to apical chloride gradient and the current was stimulated by consecutive addition of 30 nM, 100 nM, 300 nM, 1 μM, 3 μM, 10 μM forskolin and 100 μM genistein followed by CFTR inhibition with 20 μM inhibitor 172 (Inh172). The inhibitor-sensitive peak current values are plotted in Fig.1f. (f) Cellular expression of ΔF508-CFTR with or without suppressor mutation and VX-809 was measured by immunoblotting in CFBE41o- cells. Na^+/K^+-ATPase (ATPase) was used as a loading control. (g) Augmented PM density of ΔF508-R1S (Res_{R1S}) and ΔF508-R1070W CFTR (Res_{R1070W}) by class-I corrector in CFBE41o- cells was calculated as in Fig.S2a. The >2 log_2 ratio of Res_{R1S} over Res_{R1070W} indicates the preferential effect of class-I correctors on the NBD1-MSD2 interface (right).

Supplementary Figure 4. C18 prevents thermal inactivation of the ΔF508-2RK CFTR channel *in vitro.*

(a-c) The effect of the 2RK mutation on the ΔF508-CFTR biochemical and functional phenotype. (a) The PM density of the CFTR constructs was measured by cell surface ELISA in BHK cells. The 2RK mutation modestly improved the ΔF508-CFTR low temperature rescue and (b) PM stability. Anti-HA Ab bound BHK cells were incubated for the indicated chase time at 37°C and the OM remaining CFTR was measured by ELISA. (c) The 2RK mutation modestly increased the functional PM stability of the rescued ΔF508 CFTR, determined by iodide efflux assay. (d) Representative gating current (~1 min) of reconstituted ΔF508-CFTR-2RK in artificial phospholipid bilayer in the presence of 3 μM C18 during the temperature ramp at ~24°C, ~30°C and ~36°C. Open probability (P_o) of CFTR was analyzed at the indicated temperature as described in Methods and summarized in Fig.2b. Two channels were incorporated into the bilayer for the experiment showing the gating

activity at 30°C and 36°C. A single channel activity from a separate experiment is shown at 24°C. The channel closed state is indicated by "c".

Supplementary Figure 5. Docking of VX-809 to the ΔF508-NBD1 crystal structure, as well as to the closed and open ΔF508 CFTR models.

(a) *In silico* docking of VX-809 was performed to the X-ray structure of NBD1 (PDBID:2BBT) to mimic corrector binding during or immediately after NBD1 translation, preceding complete domain-domain assembly. Solubilizing mutations in the 2BBT structure were reverted to WT (see details in Methods). In the simulation using this NBD1 structure, VX-809 is bound to the isolated NBD1 at the CL1/4 or the NBD2 interface. Views from three different orientations are presented. The cytosolic loops (CL1 and CL4) are shown for comparison to the full-length CFTR model. Clusters are depicted in mesh representation to indicate their volume. Red, blue, magenta, and cyan of VX-809 clusters represent increasing binding free energy with the corresponding color number specifying the domain binding. The size of individual clusters and their average binding energy can be found in Supplementary Table 3. The CFTR binding sites were determined using PyMOL (http://www.pymol.org) by selecting amino acids in less than 4 Å distance from every molecule in each cluster. (b) For *in silico* docking to ΔF508 CFTR the search space includes NBD1, NBD2 and major parts of CL1-4. The grid box is depicted on the closed CFTR model. Color-coding is the same as in panel a and Fig.1a. (c-f) *In silico* docking of the VX-809 to the closed and open ΔF508 CFTR models. VX-809 primary binding is indicated as site I at the CL1/4-NBD1/2 interface in the full-length closed and open molecules (c, e, and Fig.2c). We further performed *in silico* docking of VX-809 to the ΔF508-CFTR-ΔNBD2 model considering that NBD2 is dispensable for the CFTR folding and that VX-809 effect was almost completely retained upon ΔNBD2 (Fig.3e-f). In closed

CFTR-ΔNBD2 an additional binding site is predicted at the β-subdomain (site II) (c-d). Moreover, the NBD1-CL1/4 interface near the ΔF508 cavity was predicted as the binding site in addition to site I and site II in the closed CFTR-ΔNBD2 model (d and f). NBD2 is hidden in the full-length model to facilitate comparison. Color-coding is the same as in Supplementary Fig.5b.

Supplementary Figure 6. The effect of NBD1-CL4 stabilization on the corrector-induced rescue of CFTR variants in BHK cells.

(a) PM density of ΔF508-CFTR-3S, ΔF508- CFTR-3S-R1070W and ΔF508-CFTR-3S-V510D was measured by cell surface ELISA in BHK cells treated with correctors for 24 h at 37°C. The same data are also plotted in Fig.3d as % of the respective DMSO controls. (b) The effect of correctors on the PM density of WT CFTR and V510D-CFTR (WT-V510D) was measured by cell surface ELISA as in panel (a). Correction efficiency was normalized for WT (left), and for the respective DMSO control (right). (c) Steady-state expression (upper) and PM density (lower) of R170G-CFTR with stabilized NBD1-MSD2 interface (V510D) or NBD1 (R1S) were examined by Western blotting and cell surface ELISA, respectively. (d) The effect of correctors on the PM density of R170G-CFTR and R170G-V510D-CFTR was measured by ELISA as in panel b. ELISA data represent means ± SEM (n=8). Cells were exposed to correctors (10 μM C3, 3 μM C18, 3 μM VX809 or 10 μM C4) for 24 h at 37°C.

Supplementary Figure 7. The effect of correctors on the expression of TM1, CL1 and CL2 CFTR mutants, CFTR domain combinations and CFTR-ΔNBD2.

(a) PM density of MSD1 CFTR mutants in the TM1 (G85E, G91R), CL1 (S168/S169A, R170G, K174A, Q179K) or CL2 (M265R, W277R) were measured by cell surface ELISA in BHK cells

treated with 3 μM VX-809 for 24 h at 37°C. (b-e) Effect of VX-809 on the steady-state expression of CFTR domain combinations was examined by Western blotting with the CFTR N-terminal tail specific MM13-4 or anti-HA Ab. VX-809 was added as in panel a. (b) Accumulation of WT and ΔF508 MSD1-NBD1 fragments was increased by VX-809. (c-d) VX-809 increased the cellular expression of the WT CFTR domains containing MSD1, but not without MSD1. The relative level of the CFTR domains quantified by densitometry is indicated. (e) Summary of the VX-809 effect on the expression of WT CFTR domain combinations. CFTR domain boundaries are indicated as amino acid residues in the primary sequence. M1, MSD1; N1, NBD1; M2, MSD2; N2, NBD2. (f-g) Effect of NBD2 deletion (ΔNBD2) on the correction of the ΔF508-CFTR-R1070W PM density (f) and cellular expression (g), measured by ELISA and Western blotting, respectively. Cells were exposed to correctors (10 μM C3, 3 μM C18, 3 μM VX809, 10 μM C4, 5 μg/ml core-corr-II or 10% glycerol) for 24 h at 37°C (f-g). All ELISA data represent means ± SEM (n=6-9).

Supplementary Figure 8. *In silico* docking of C4 to the ΔF508-NBD1 crystal structure (a), closed (b-c) and open (d-e) ΔF508-CFTR models.

In the full-length CFTR models, C4 was predicted to bind to site I at the MSD1/2-NBD1/2 interface, site II and III at the NBD1-NBD2 interface and near regulatory insertion (site RI) (b and d). C4 putative binding, however, was diminished at both sites I and RI in the closed CFTR-ΔNBD2 model, as well as at sites II and III in the open CFTR-ΔNBD2 model. C4 binding, however, was detected at site I in the open CFTR-ΔNBD2 model (c and e). Considering that the NBD2 was indispensable for the C4 rescue effect (Fig.3e-f and Supplementary Fig.7f-g), site II and site III likely represent functionally relevant binding sites for the C4. The RI region could be ruled out as a relevant C4 binding site for rescue, since deletion of the RI region largely preserved the C4

rescue effect of the ΔF508-CFTR-ΔRI (Supplementary Fig.9f). Color-coding is as defined in Supplementary Fig.5.

Supplementary Figure 9. In silico docking of core-corr-II to the ΔF508-NBD1 crystal structure, as well as to the closed and open ΔF508-CFTR models.

(a) Core-corr-II, similar to VX-809 and C4, is docked to the NBD1 binding cavity of the CL4. (b) In the closed CFTR model, core-corr-II binds to sites I, II and RI. (c) These interactions are either weakened or disappeared in the absence of NBD2. (d-e) In the open CFTR model, core-corr-II binds to site II and partially to site I. (e) Core-corr-II association with site II is abolished in the CFTR-ΔNBD2 model. Color-coding is as in Supplementary Fig.5. According *to in silico* docking, C4 and core-corr-II are bound to NBD1 at the CL1/4 or the NBD2 interface similar to VX-809 (a and Supplementary Fig.8a). However, the binding free energies of C4 and core-corr-II were higher than that of VX-809 (-8.4 and -7.8 compared to -9.9 kcal/mol, respectively; see Supplementary Table 3), consistent with the observation that the C4 and core-corr-II rescue efficiency was lower than VX-809. Notably, the docking algorithm is sensitive enough on the homology models to yield preferential binding to the CL1/4 and not to the symmetrical CL2/3-NBD2 interface region and explains, at least in part, the differences in the molecular mechanism of CFTR variants rescue by VX-809, C4, and core-corr-II. (f) Class-II correctors binding to the Regulatory Insertion (RI) cannot account for the rescue effect since deletion of the RI (ΔRI) does not diminish the corrector rescue efficiency. The steady-state expression (upper panel) and PM density (lower panel) were determined by immunoblotting and ELISA, respectively, (n=6-9, ± SEM). Cells were exposed to correctors (10 μM C3, 3 μM C18, 3 μM VX809, 10 μM C4, 5 μg/ml core-corr-II or 10% glycerol) for 24 h at 37°C.

Supplementary Figure 10. Effect of correctors on the isolated NBD1 stability *in vitro*.

(a) Melting temperature (T_m) of isolated human ΔF508-NBD1-1S was measured *in vitro* by differential scanning fluorimetry (DSF)[26]. WT-NBD1-1S was used as a positive control. The indicated correctors or chemical chaperones (CC) (see Supplementary Table 1) were included during thermal unfolding at the following two concentrations: 3 μM and 10 μM C1, C2, C3, C4, C5, C6, C7, C9, C11, C12, C13, C14, C17, CoPo, 10 μM and 20 μM C8, C15, C16, 1 μM and 3 μM C18, VX-809, 5 μM and 15 μM RDR1, 2.5 μg/ml and 5 μg/ml core-corr-II, 5% and 10% glycerol, 150 mM and 300 mM TMAO, taurine, myo-inositol and D-sorbitol. Thermal unfolding scans of ΔF508-NBD1-1S in the presence of selected correctors are shown in Fig.4a. Data represent means ± SEM (n=3). Statistically significant change in T_m was considered larger than mean ± 3SD of DMSO treated ΔF508-NBD1-1S (34.1 ± 1.5°C). The inset indicates the ΔF508-NBD1-1S T_m elevation as a function of increasing ATP concentration. (b) Effect of C11 on the *in vitro* ubiquitination of WT or ΔF508-NBD1-1S by CHIP was analyzed by Western blotting with anti-NBD1 (L12B4) antibody as previously[26]. (c) Representative mass spectra of singly charged peptides after 5 min labelling with D_2O; ^{505}NIIF^{508} (NIIF + H^+ = 506.30) of wt NBD1-1S (left panel) and ^{505}NIIG^{509} (NIIG + H^+ = 416.25) of ΔF508-NBD1-1S (right panel) at 22 °C. Theoretical monoisotopic masses of singly charged peptides are shown.

Supplementary Figure 11. ΔF508-CFTR rescue by corrector combination in MDCKII and NCI-H441 polarized epithelia.

(a, b) PM density (a) and steady-state expression (b) of ΔF508-CFTR in MDCKII cells were measured by ELISA (n=8) and Western blotting, respectively. Correctors were added with or without 5% or 10% glycerol (Gly) at 37°C for 24 h. The same concentration of correctors were used

in both panels. Low temperature (26°C) rescued ΔF508-CFTR (rΔF) was used as a positive control. (c) PM density of ΔF508-CFTR in NCI-H441 Tet-on cells (n=8). Data represent means ± SEM. (d) Corrector combination synergistically rescues the ΔF508-CFTR in MDCKII and NCI-H441 Tet-On epithelial cells. PM density of cells treated with VX-809 (3 μM) or corrector combination (3 μM VX-809, 10 μM C4 and 5% glycerol [Gly]) was determined by cell surface ELISA (n=6-16).

Supplementary Figure 12. Effect of correctors on WT CFTR PM expression in BHK cells. (a) PM density of WT CFTR was measured by cell surface ELISA in BHK cells treated with correctors (10 μM C3, 10 μM C4, 3 μM C18, 3 μM VX-809 or 10% glycerol) at 37°C for 24 h. (b) Effect of second-site suppressor mutations on the corrector efficacy on WT expression was determined by PM ELISA. Correctors were added as in panel a. Data represent means ± SEM (n=8). (c) Comparison of VX-809 in silico docking to WT and ΔF508 CFTR closed conformation. Docking and analysis was performed as described in Methods. The poses of VX-809 with the lowest energies (red) occupy the site I as in the case of the ΔF508 CFTR (right; see also Fig.S5c). A low energy cluster (magenta) in the WT partially overlaps with two low energy clusters (blue and turquoise) in the ΔF508 CFTR. At the back of RI and the β-subdomain an additional docking site appears (turquoise) in the WT. These results suggest that the targets of VX-809 are partially overlap in the WT and ΔF508 CFTR.

Supplementary Figure 13. Full size views of autoradiographs and western blot films displayed in cropped formats in Figures 1, 3, 5 and 6, as well as Supplementary Figs. 2 and 3 as indicated nearby each panel.

Supplementary Figure 1

a

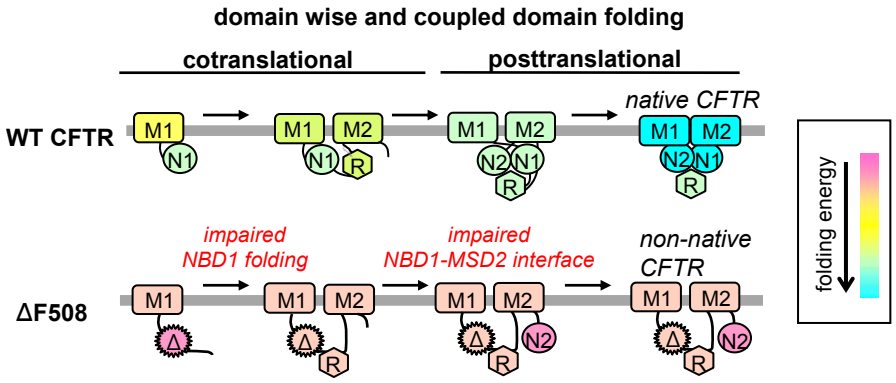

b

maneuver	Primary folding defect		rescue effect
	NBD1	NBD1-MSD2 interface	
second site suppressor mutation (genetic rescue)	3S, R1S	-	<20%
	-	R1070W, V510D	5-10%
	3S, R1S	R1070W, V510D	~80%
corrector (pharmacological rescue)	*corrector A*	-	<5%
	-	*corrector B*	<10%
	corrector A	*corrector B*	*~80% ?*
structure-based corrector screening	*corrector A*	R1070W	*50-80% ?*
	3S, R1S	*corrector B*	*50-80% ?*

Supplementary Figure 2

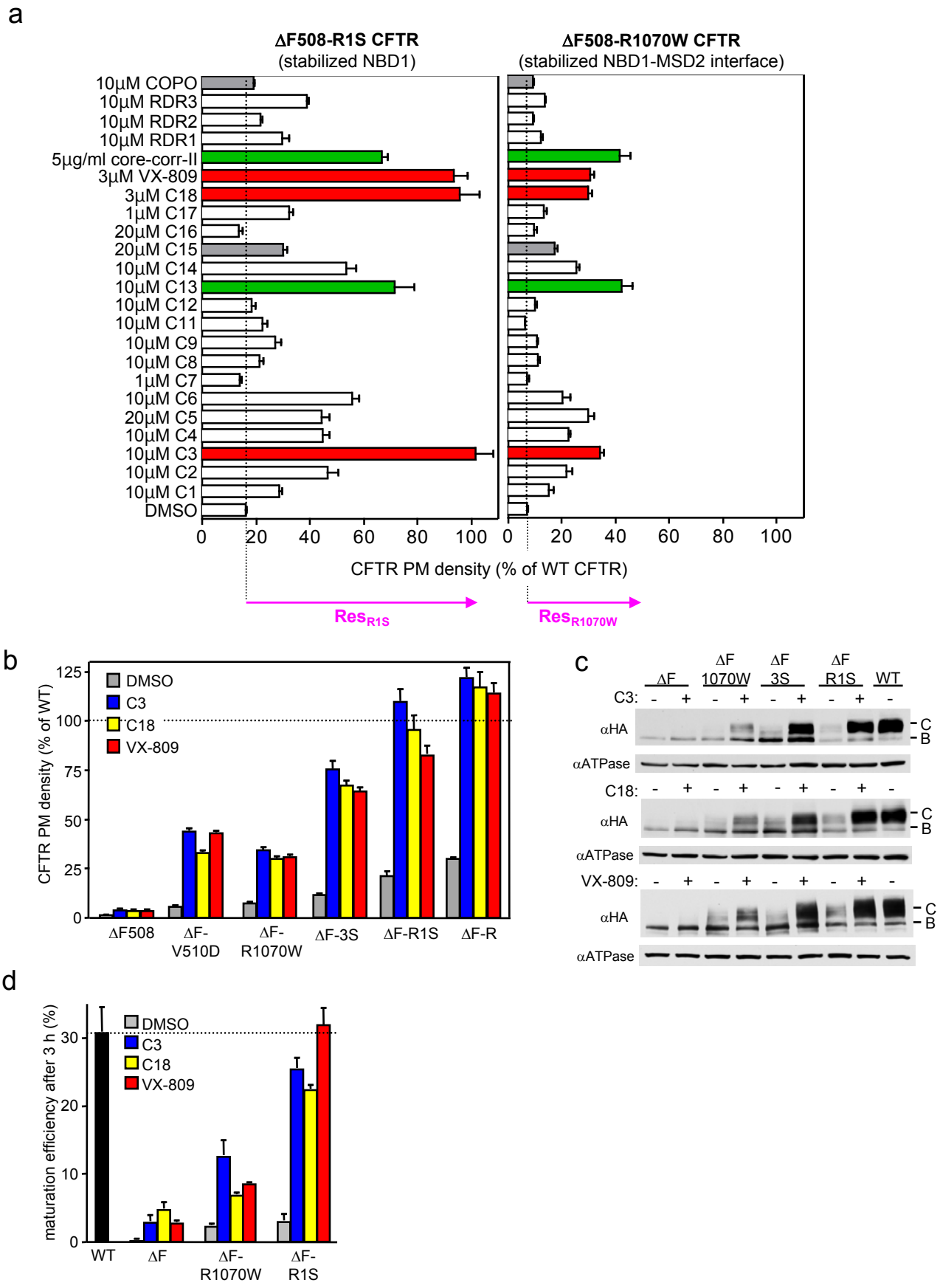

Supplementary Figure 3

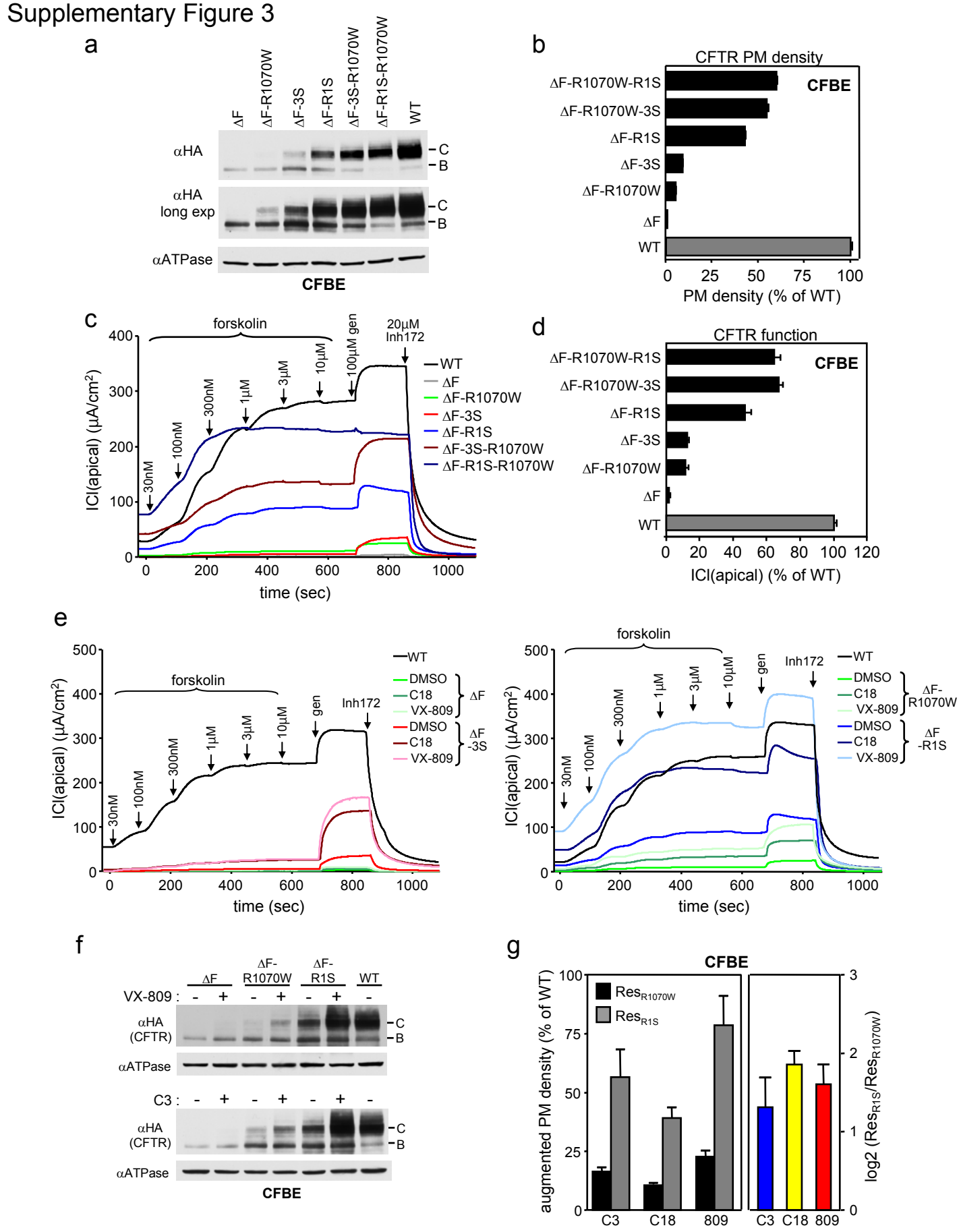

Supplementary Figure 4

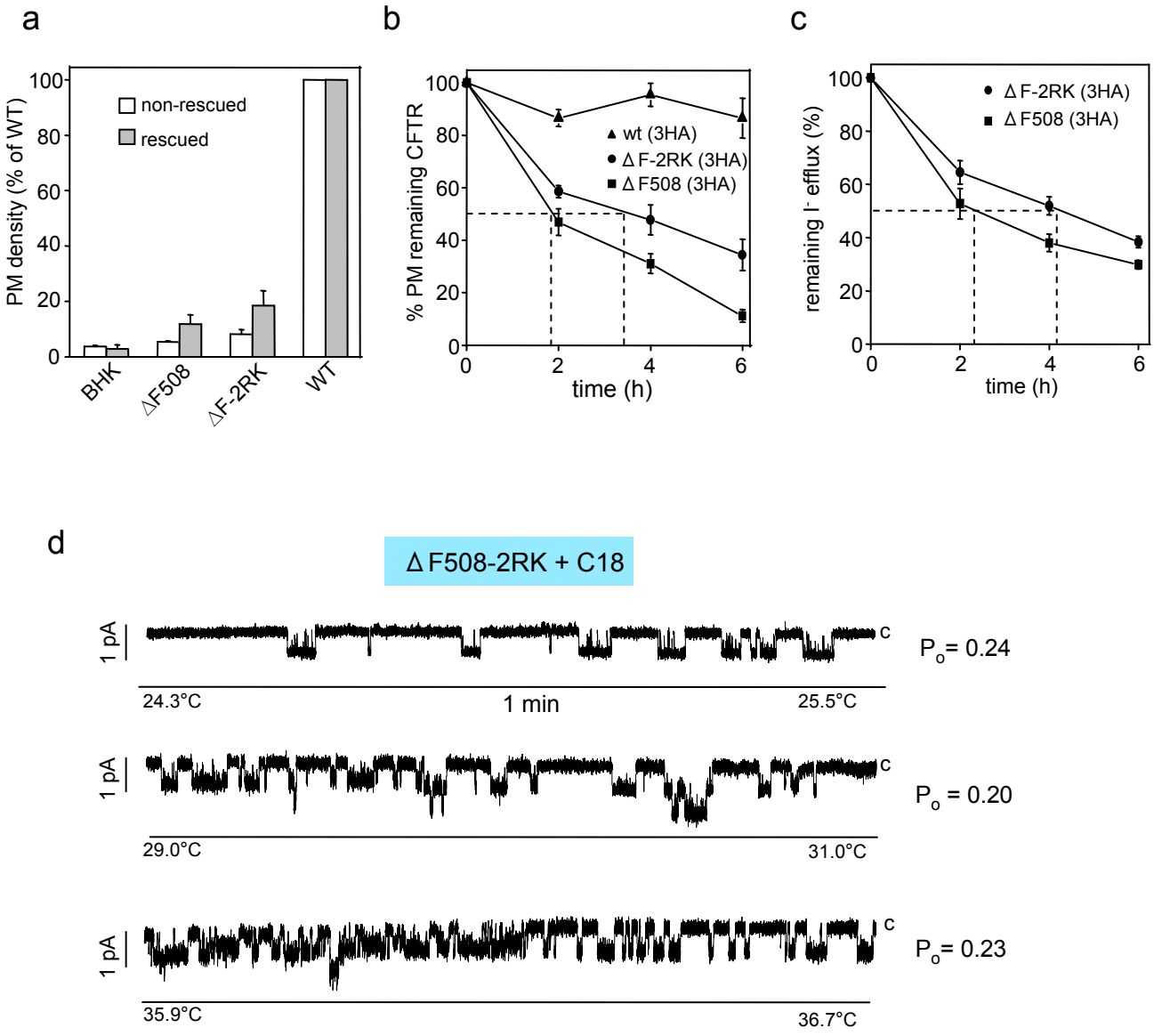

Supplementary Figure 5

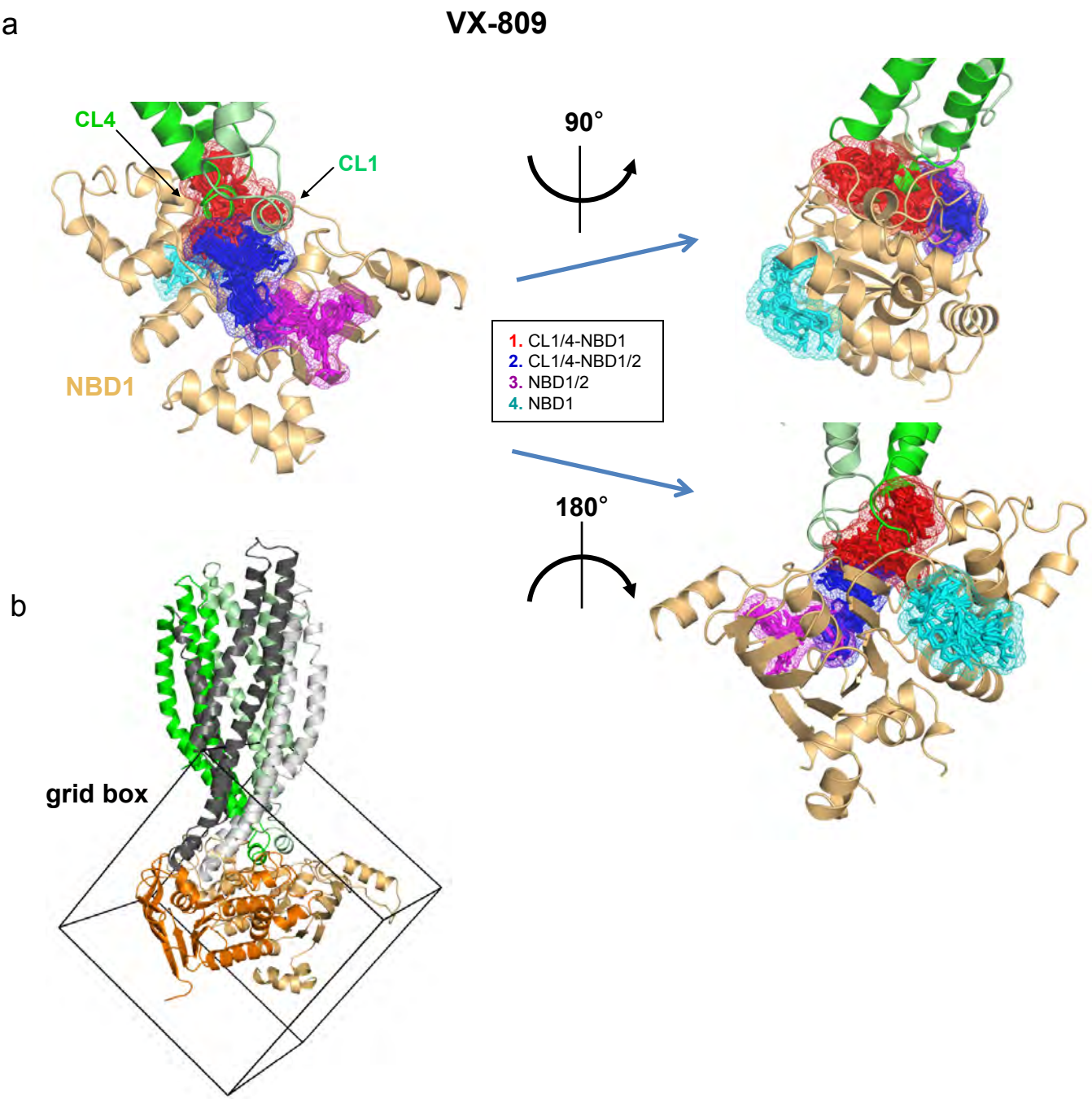

Supplementary Figure 5 - continued

VX-809

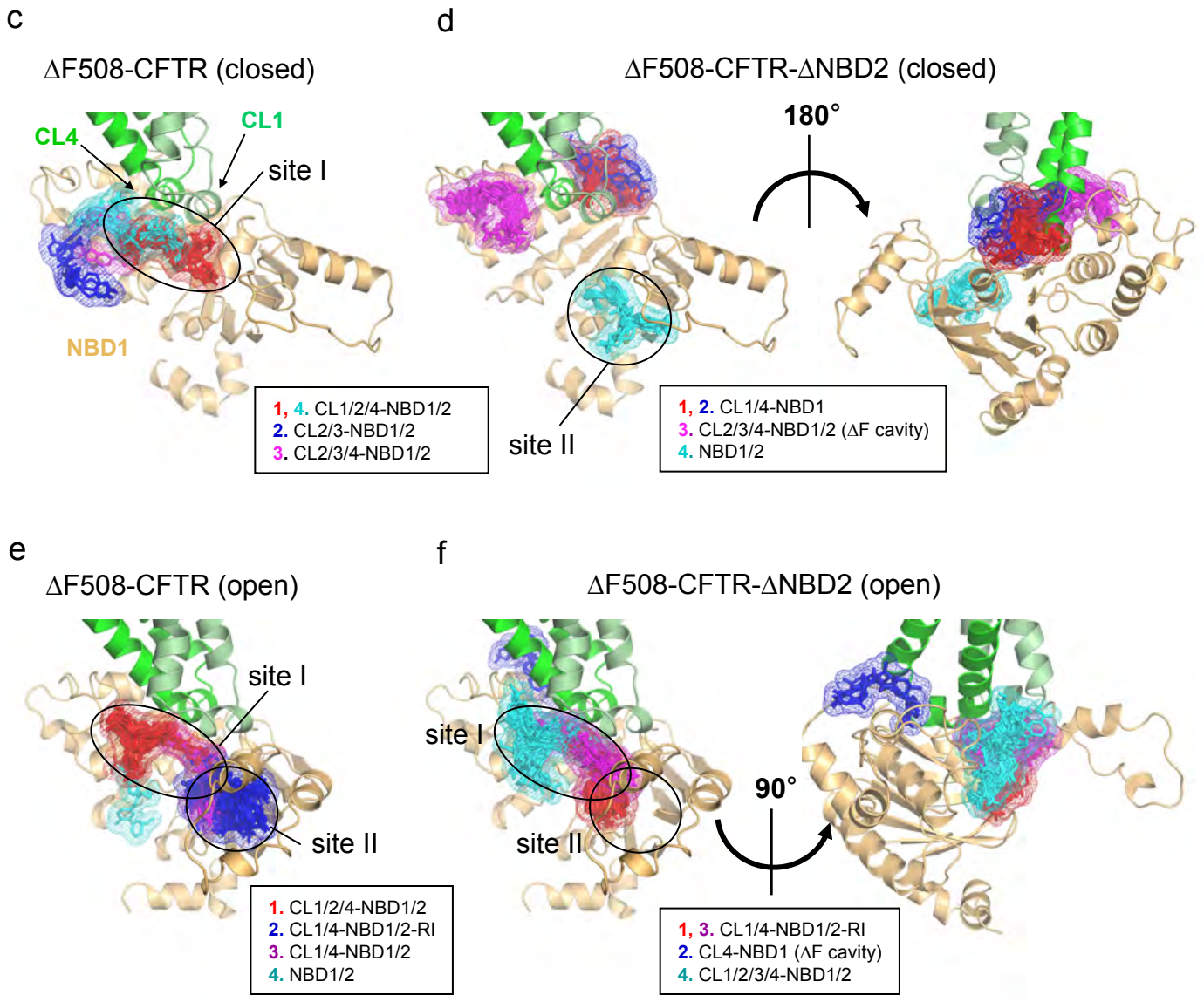

Supplementary Figure 6

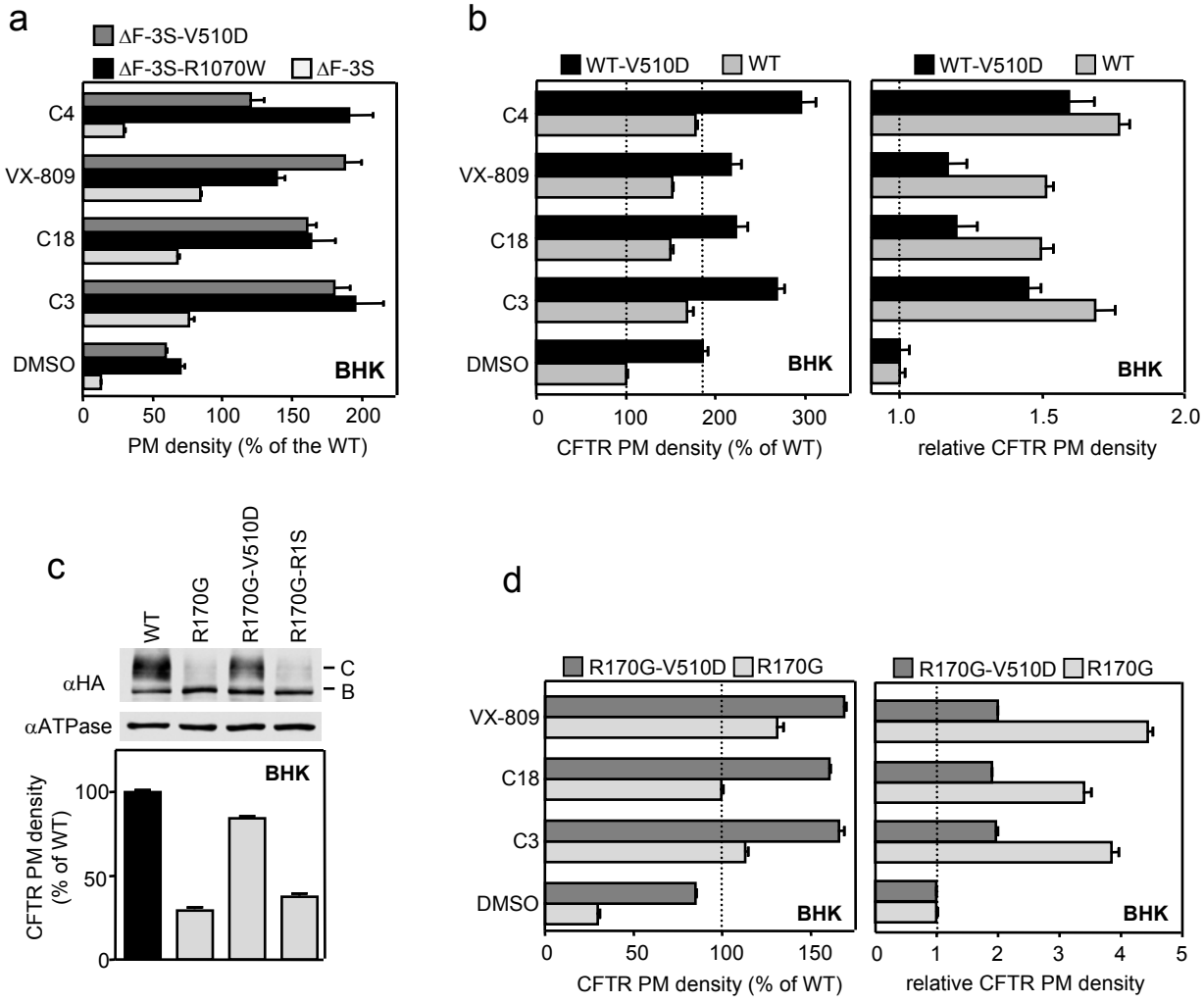

Supplementary Figure 7

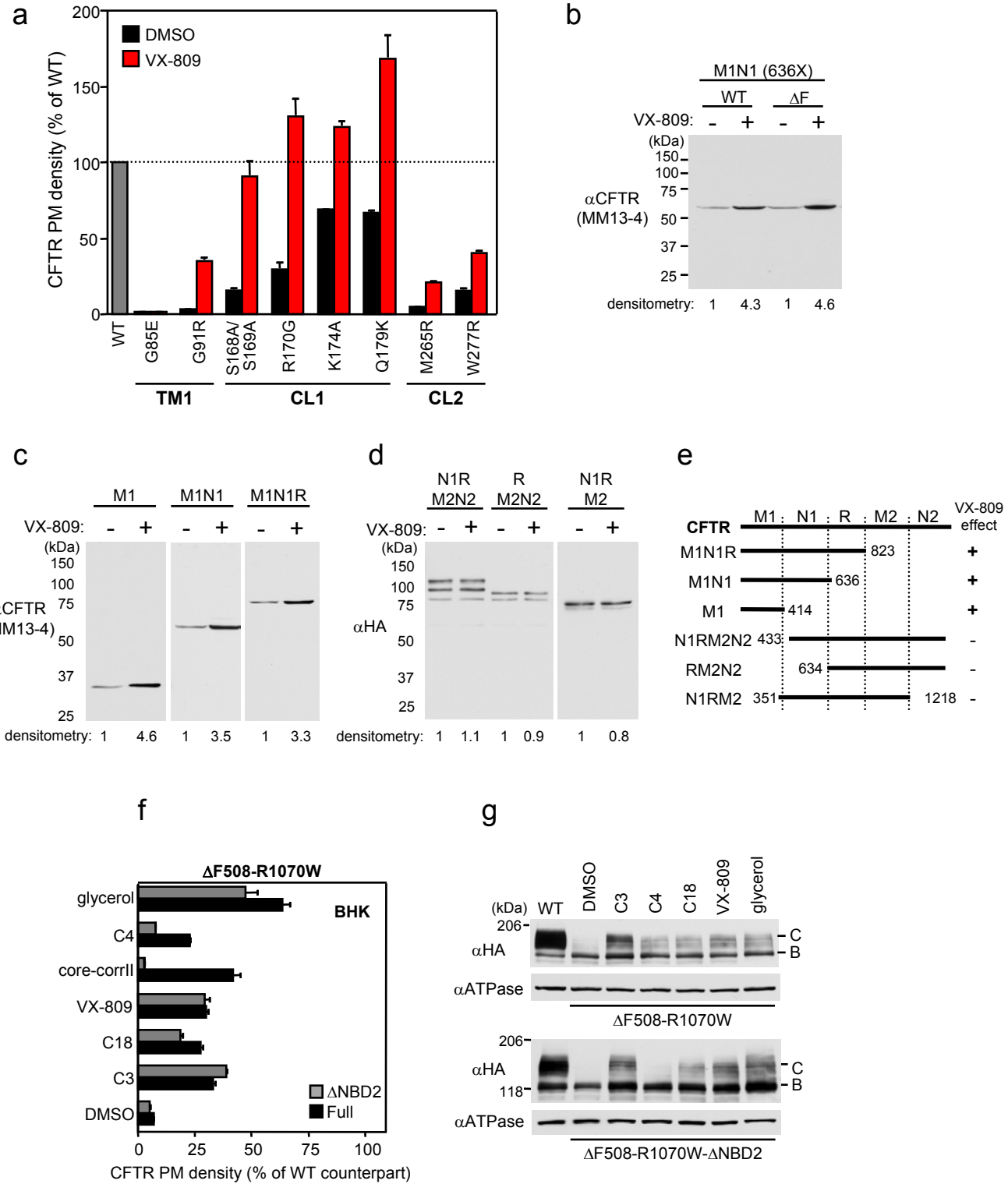

Supplementary Figure 8

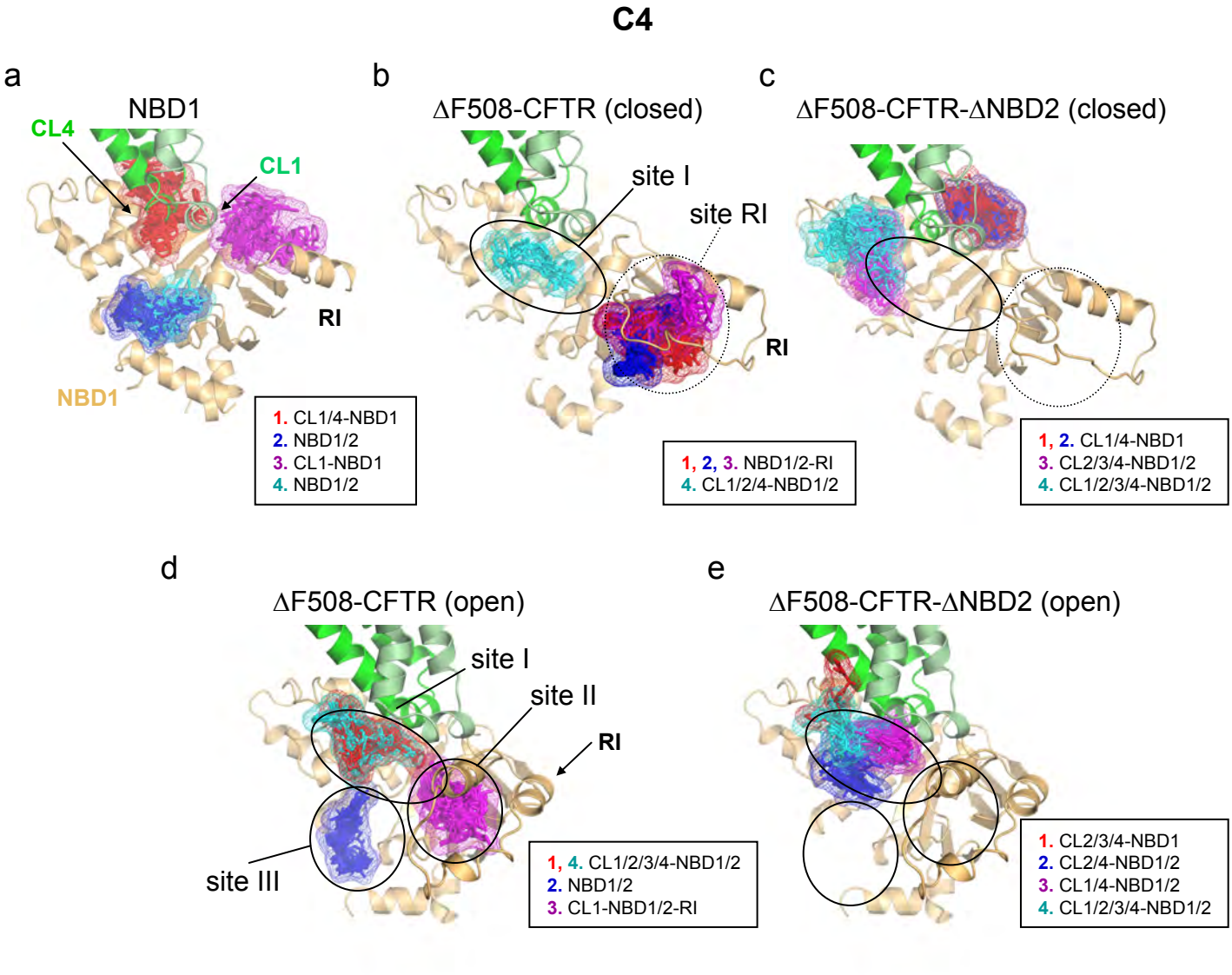

Supplementary Figure 9

core-corr-II

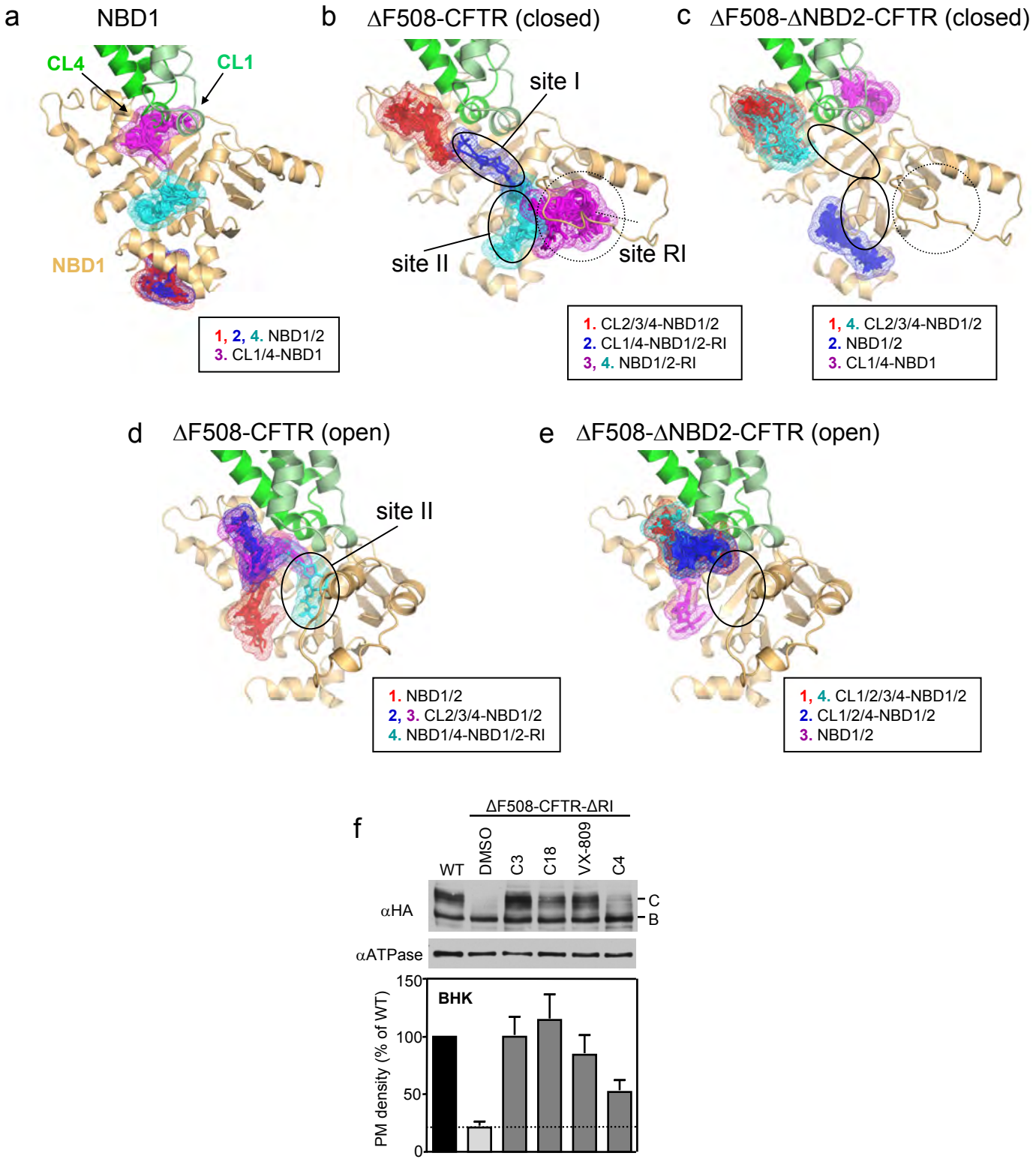

Supplementary Figure 10

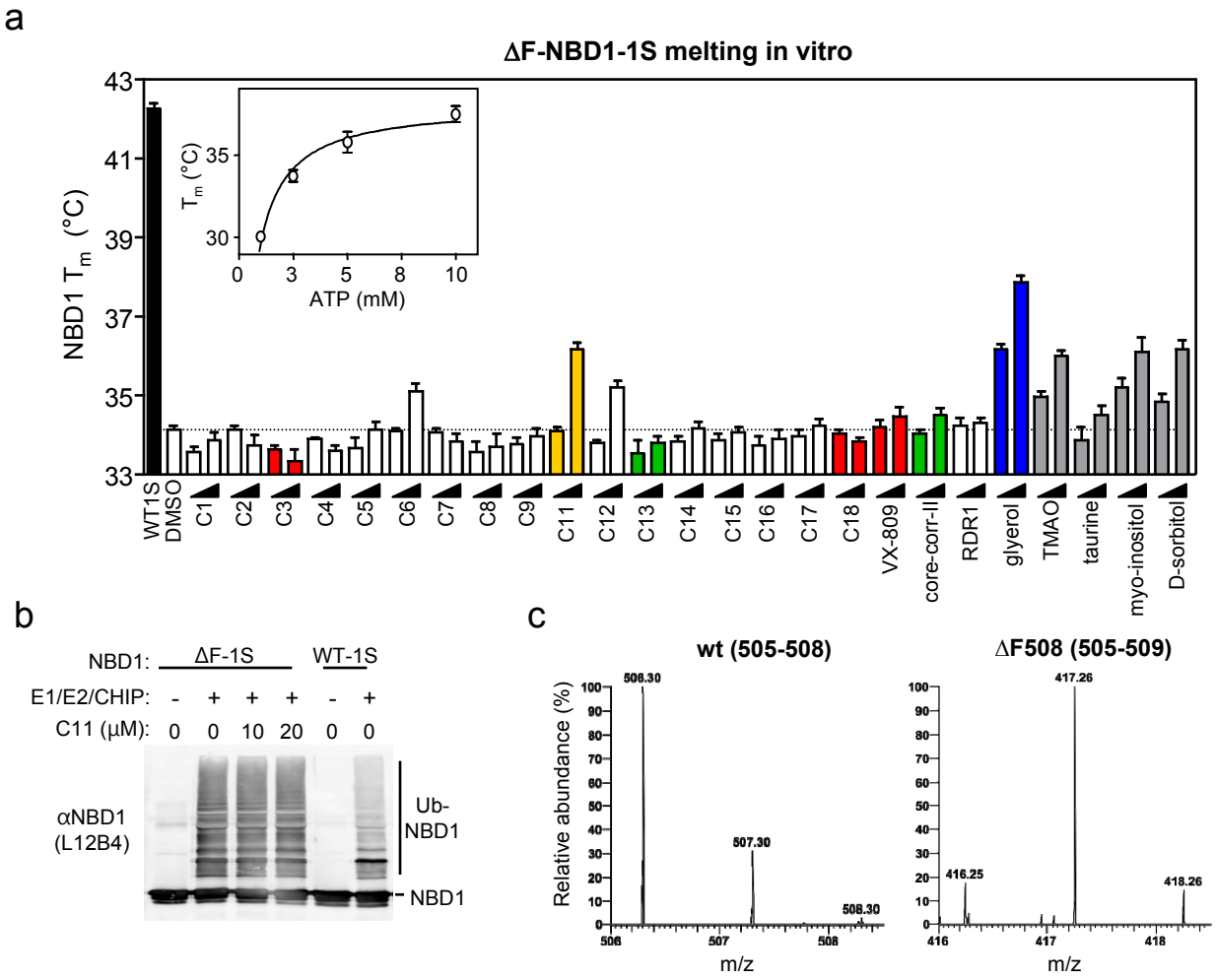

Supplementary Figure 11

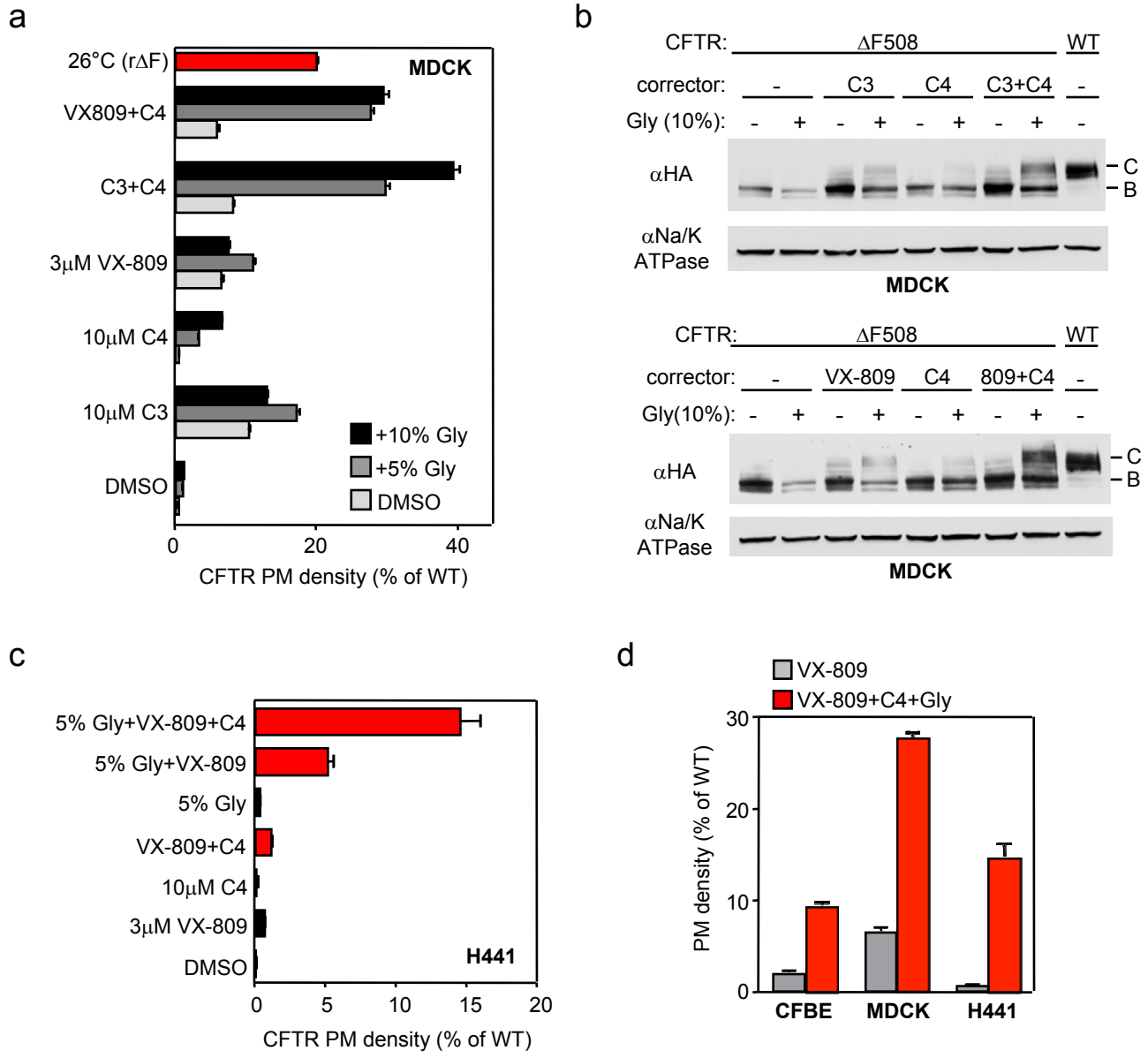

Supplementary Figure 12

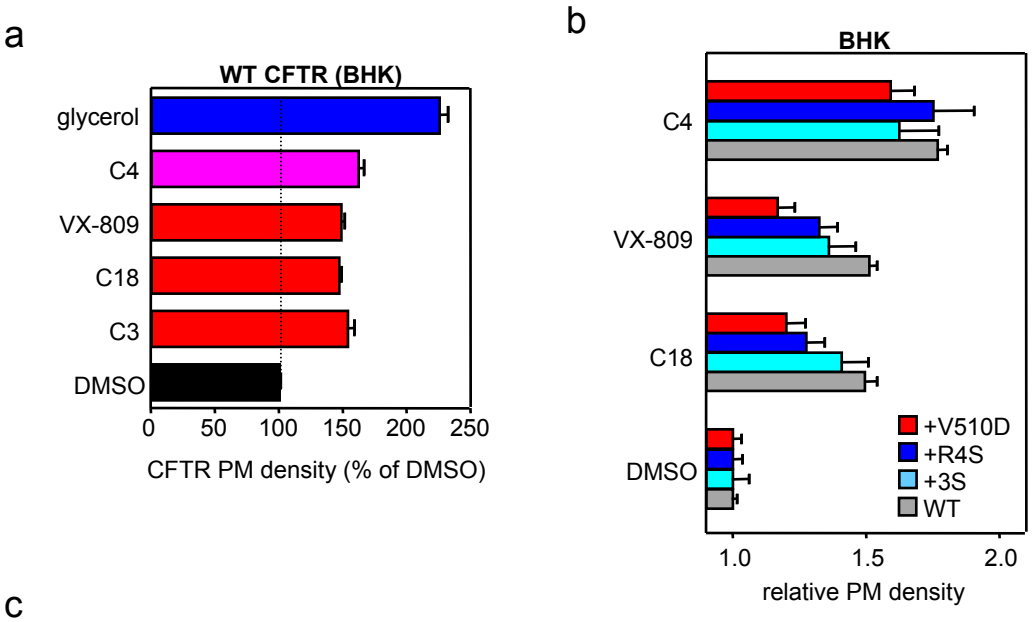

c

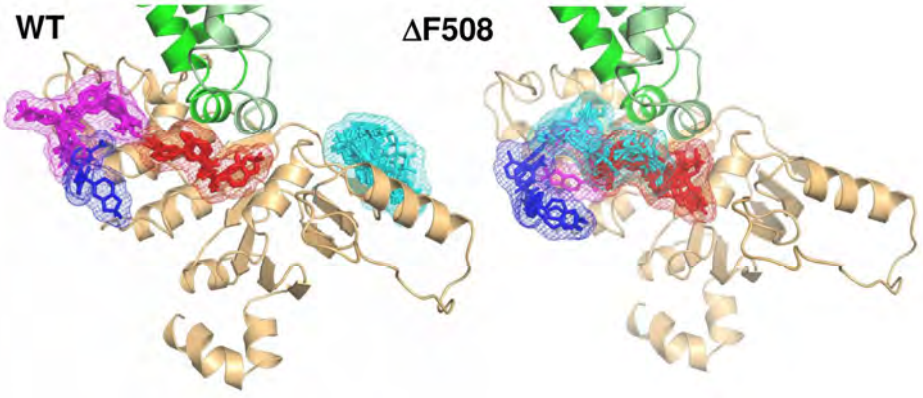

Supplementary Figure 13

Fig.1d

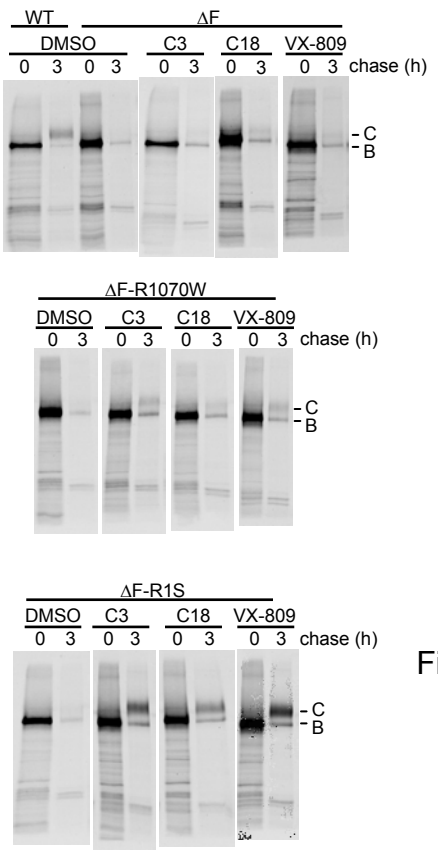

Fig.3a

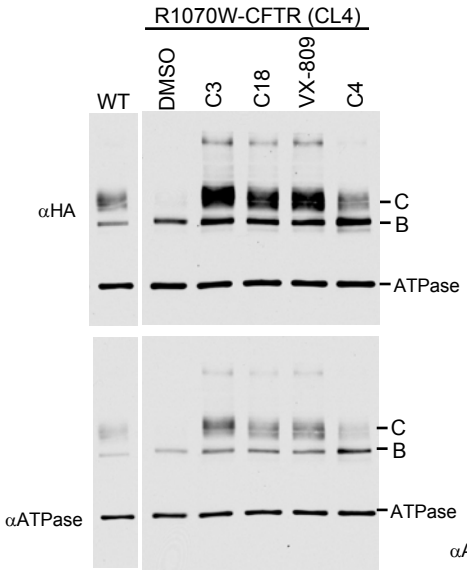

Fig.3b

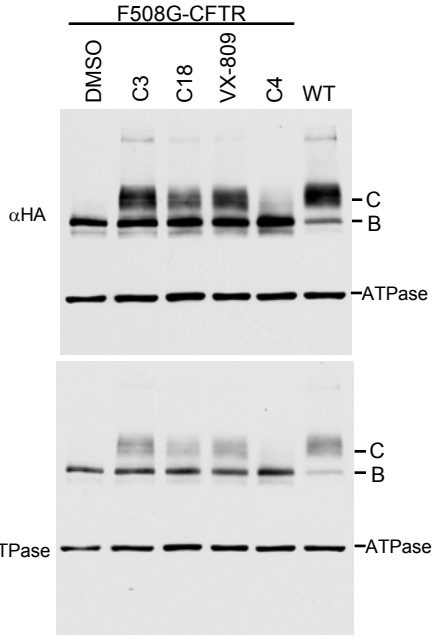

Fig.3c

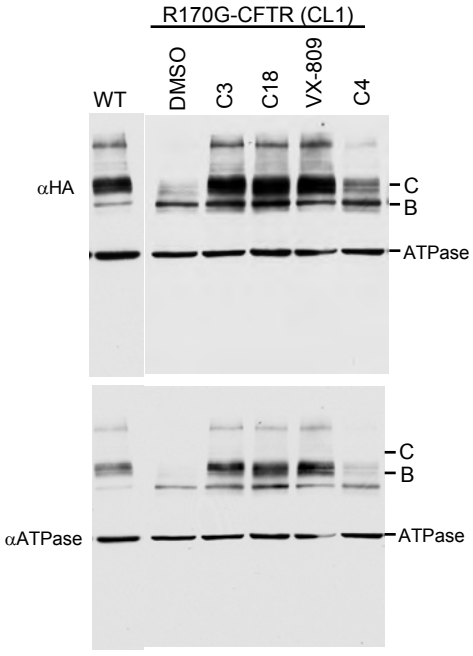

Fig.3f

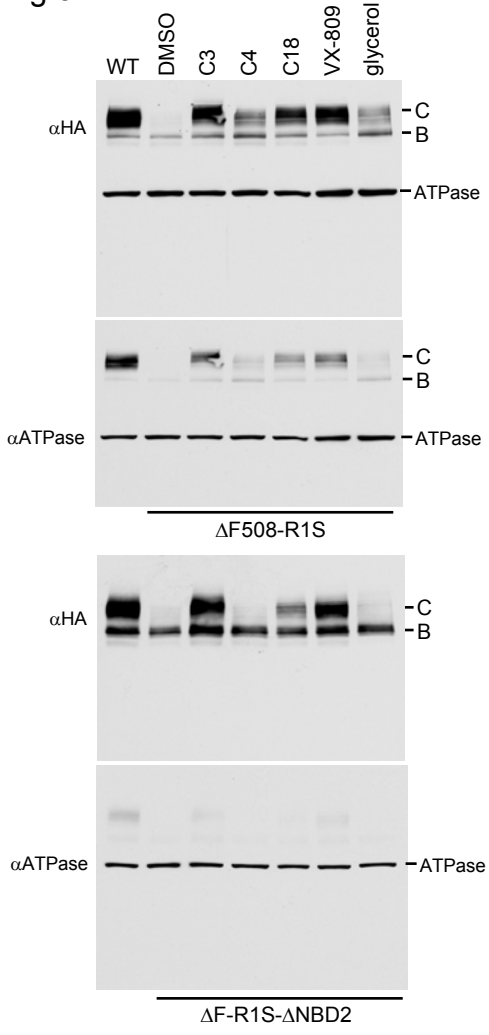

Supplementary Figure 13 - continued

Fig.5c

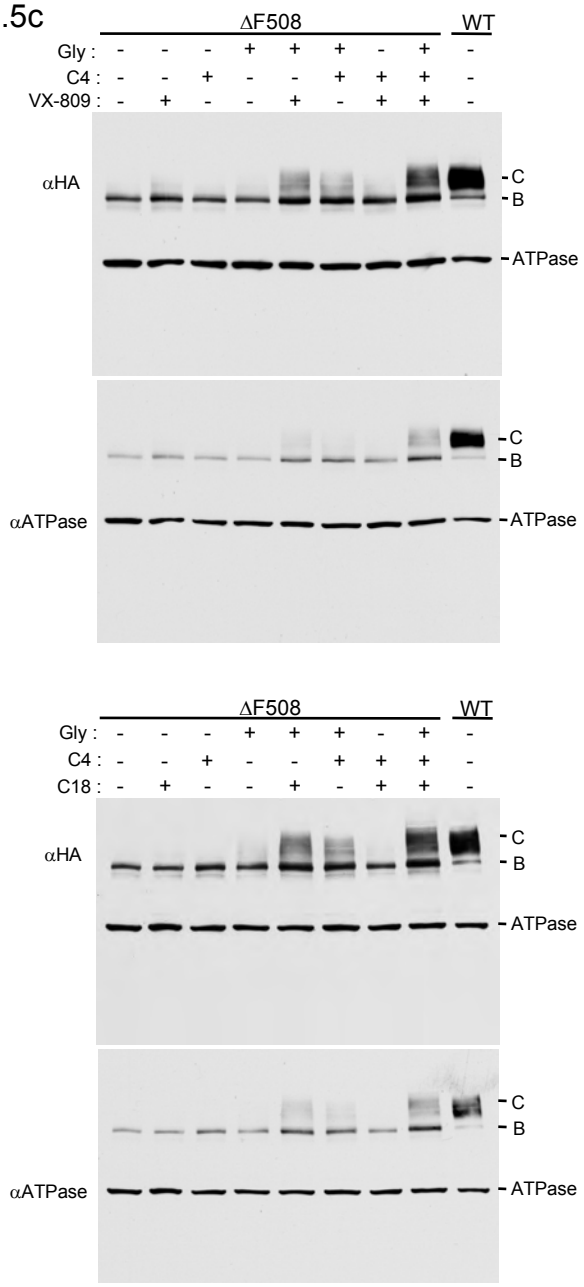

Fig.5d

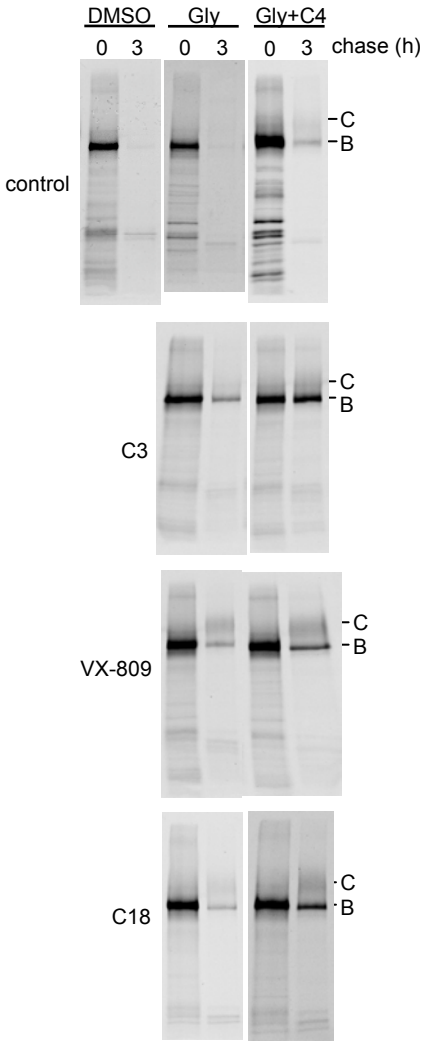

Fig.6b top

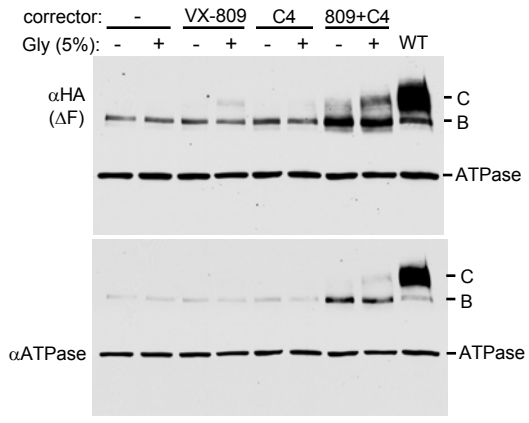

Fig.6b bottom

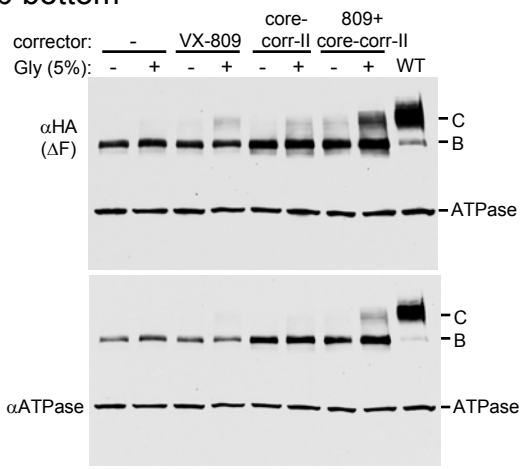

Supplementary Figure S13 - continued

Fig.S2c

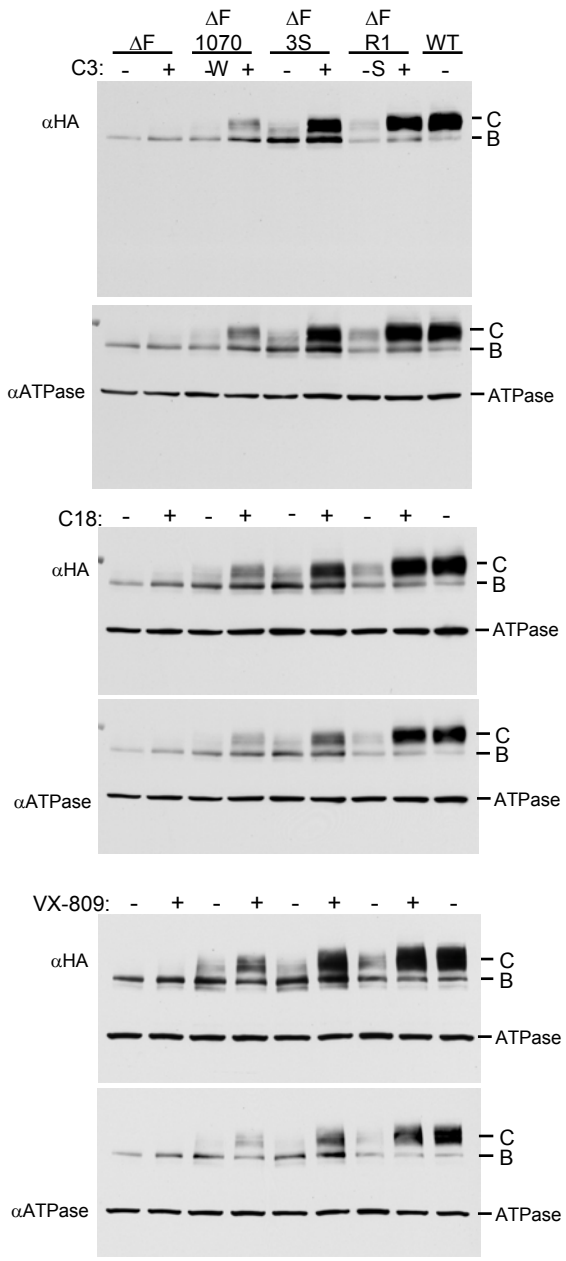

Fig.S3a

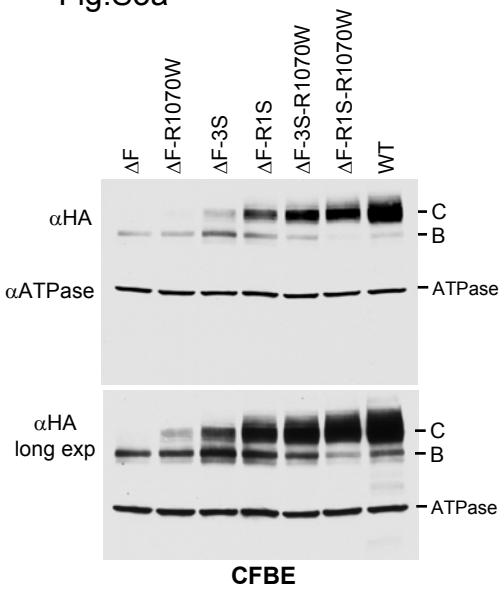

Fig.S3f (1g)

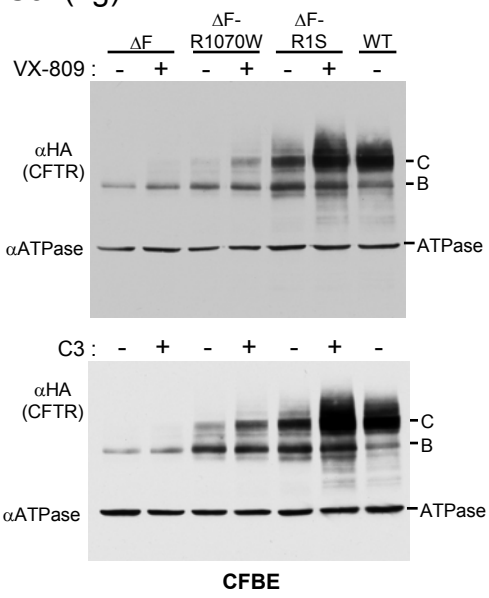

Supplementary Table 1

CFTR correctors and chemical chaperones used in this study

The terminology of corrector use in this study was defined according to that specified in the Cystic Fibrosis Foundation Therapeutics (CFFT) CFTR modulator set.

corrector	other name	chemical name	source
C1		6-(1H-Benzoimidazol-2-ylsulfanylmethyl)-2-(6-methoxy-4-methyl-quinazolin-2-ylamino)-pyrimidin-4-ol	CFFT
C2	VRT-640	2-{1-[4-(4-Chloro-benzensulfonyl)-piperazin-1-yl]-ethyl}-4-piperidin-1-yl-quinazoline	CFFT
C3	VRT-325	4-Cyclohexyloxy-2-{1-[4-(4-methoxy-benzensulfonyl)-piperazin-1-yl]-ethyl}-quinazoline	CFFT
C4	corr-4a	N-[2-(5-Chloro-2-methoxy-phenylamino)-4'-methyl-[4,5']bithiazolyl-2'-yl]-benzamide	CFFT
C5	corr-5a	4,5,7-trimethyl-N-phenylquinolin-2-amine	CFFT
C6	corr-5c	N-(4-bromophenyl)-4-methylquinolin-2-amine	CFFT
C7	Genzyme cmpd 48	2-(4-isopropoxypicolinoyl)-N-(4-pentylphenyl)-1,2,3,4-tetrahydroisoquinoline-3-carboxamide	CFFT
C8		N-(2-fluorophenyl)-2-(1H-indol-3-yl)-2-oxoacetamide	CFFT
C9	KM11060	7-chloro-4-(4-(4-chlorophenylsulfonyl)piperazin-1-yl)quinoline	CFFT
C11	Dynasore	(Z)-N'-(3,4-dihydroxybenzylidene)-3-hydroxy-2-naphthohydrazide	CFFT
C12	corr-2i	N-(4-fluorophenyl)-4-p-tolylthiazol-2-amine	CFFT
C13	corr-4c	N-(2-(3-acetylphenylamino)-4'-methyl-4,5'-bithiazol-2'-yl)benzamide	CFFT
C14	corr-4d	N-(2'-(2-methoxyphenylamino)-4-methyl-5,5'-bithiazol-2-yl)benzamide	CFFT
C15	corr-2b	N-phenyl-4-(4-vinylphenyl)thiazol-2-amine	CFFT
C16	corr-3d	2-(6-methoxy-4-methylquinazolin-2-ylamino)-5,6-dimethylpyrimidin-4(1H)-one	CFFT
C17	15jf	N-(2-(5-chloro-2-methoxyphenylamino)-4'-methyl-4,5'-bithiazol-2'-yl)pivalamide	CFFT
C18	CF-106951	1-(benzo[d][1,3]dioxol-5-yl)-N-(5-((2-chlorophenyl)(3-hydroxypyrrolidin-1-yl)methyl)thiazol-2-yl)cyclopropanecarboxamide	CFFT
VX-809		3-{6-{[1-(2,2-difluoro-1,3-benzodioxol-5-yl)cyclopropanecarbonyl]amino}-3-methylpyridin-2-yl}benzoic acid	Selleck Chemicals
core-corr-II		N-(8-((5-chloro-2-methoxyphenyl)amino)-5,6-dihydro-4H-cyclohepta[1,2-d:3,4-d']bis(thiazole)-2-yl)pivalamide	Mark Kurth, UC Davis
RDR1		5-(4-nitrophenyl)-2-furaldehyde 2-phenylhydrazone	David Thomas, McGill
RDR2		5-(4-nitrophenyl)-2-furaldehyde 2-methylhydrazone	David Thomas, McGill
RDR3		5-(2-{[5-(2-bromo-4-nitrophenyl)-2-furyl]methylene}hydrazino)-2-chlorobenzoic acid	David Thomas, McGill
CoPo-22		N-(2-((3-Cyano-5,7-dimethylquinolin-2-yl)amino)ethyl)-3-methoxybenzamide	Alan Verkman, UCSF
Chemical chaperone			**source**
glycerol			Sigma
TMAO (Trimethylamine N-oxide)			Sigma
taurine			Sigma
myo-inositol			Sigma
D-sorbitol			Sigma

Supplementary Table 2
CFTR mutants used in this study

NBD1 mutants

mutant	mutation	Tm of the isolated NBD1
WT CFTR (0S)	None	39.8 ± 0.2°C
1S	F494N	41.8 ± 0.2°C
3S	F494N, Q637R, F429S	44.1 ± 0.3°C
R1S	G550E, R553Q, R555K, F494N	40.2 ± 0.1°C
R4S	G550E, R553Q, R555K, F409L, F429S, F433L, H667R	45.9 ± 0.1°C
V510D	V510D	42.7 ± 0.2°C
F508G	F508G	38.3 ± 0.1°C
ΔF508	ΔF508	31.7 ± 0.1°C
ΔF508-1S	ΔF508, F494N	33.2 ± 0.3°C
ΔF508-3S	ΔF508, F494N, Q637R, F429S	37.4 ± 0.2°C
ΔF508-R	ΔF508, G550E, R553Q, R555K	37.0 ± 0.1°C
ΔF508-R1S	ΔF508, G550E, R553Q, R555K, F494N	40.7 ± 0.2°C
ΔF508-R4S	ΔF508, G550E, R553Q, R555K, F409L, F429S, F433L, H667R	39.8 ± 0.1°C
ΔF508-V510D	ΔF508, V510D	34.9 ± 0.5°C
ΔF508-ΔRI	ΔF508, deletion of amino acid 404-435 (RI)	42.5 ± 0.5°C

Domain interface or other mutants

mutant	mutation	domain
R1070W	R1070W	MSD2 (CL4)
R170G	R170G	MSD1 (CL1)
R170G-V510D	R170G, V510D	MSD1 (CL1) & NBD1
R170G-R1S	R170G, G550E, R553Q, R555K, F494N	MSD1 (CL1) & NBD1
1218X	deletion of amino acid after 1218	NBD2
ΔF508-R1070W	ΔF508, R1070W	MSD2 (CL4)
ΔF508-1S-R1070W	ΔF508, F494N, R1070W	NBD1 & MSD2 (CL4)
ΔF508-3S-R1070W	ΔF508, F494N, Q637R, F429S, R1070W	NBD1 & MSD2 (CL4)
ΔF508-R1S-R1070W	ΔF508, G550E, R553Q, R555K, F494N, R1070W	NBD1 & MSD2 (CL4)
ΔF508-3S-V510D	ΔF508, F494N, Q637R, F429S, V510D	NBD1
ΔF508-1218X	ΔF508, deletion of amino acid after 1218	NBD1 & NBD2
ΔF508-R1070W-1218X	ΔF508, R1070W, deletion of amino acid after 1218	NBD1, MSD2 (CL4) & NBD2
ΔF508-R1S-1218X	ΔF508, G550E, R553Q, R555K, F494N, deletion of amino acid after 1218	NBD1 & NBD2
ΔF508-2RK	ΔF508, R29K, R555K	N-terminal region & NBD1
G85E	G85E	MSD1 (TM1)
G91R	G91R	MSD1 (TM1)
S168A/S169A	S168A, S169A	MSD1 (CL1)
K174A	K174A	MSD1 (CL1)
Q179K	Q179K	MSD1 (CL1)
M265R	M265R	MSD1 (CL2)
W277R	W277R	MSD1 (CL2)

Supplementary Table 3
Relative binding energies of VX-809, C4 and core-corr-II

Cluster #	n(poses)[1]	E_{min}[2]	E_{ave}[3]
VX-809			
NBD1 *394 out of 750 poses in the 4 out of 41 clusters*			
1	235	-9.88	-8.565
2	125	-9.55	-8.846
3	22	-9.53	-8.778
4	12	-8.95	-8.032
full length (closed) *52 out of 750 poses in the 4 out of 79 clusters*			
1	25	-11.33	-10.246
2	3	-10.94	-9.93
3	2	-10.79	-10.765
4	22	-10.36	-9.366
ΔNBD2 *124 out of 750 poses in the 4 out of 91 clusters*			
1	52	-10.11	-9.046
2	4	-9.8	-8.495
3	39	-9.76	-8.267
4	29	-9.39	-8.695
C4			
NBD1 *223 out of 750 poses in the 4 out of 55 clusters*			
1	109	-8.43	-6.851
2	42	-8.36	-6.753
3	58	-8.3	-7.081
4	14	-8.09	-7.076
full length (closed) *130 out of 750 poses in the 4 out of 90 clusters*			
1	41	-10.7	-8.463
2	55	-10.43	-9.757
3	26	-10.15	-7.927
4	8	-10.12	-9.136
ΔNBD2 *139 out of 750 poses in the 4 out of 69 clusters*			
1	47	-8.93	-8.045
2	33	-8.64	-7.825
3	10	-8.15	-6.985
4	49	-8.08	-7.145
core-corr-II			
NBD1 *202 out of 750 poses in the 4 out of 66 clusters*			
1	19	-7.75	-7.206
2	14	-7.71	-7.299
3	123	-7.7	-7.158
4	46	-7.68	-7.003
full length (closed) *138 out of 750 poses in the 4 out of 68 clusters*			
1	53	-10.4	-9.5
2	2	-10.34	-10.265
3	34	-9.83	-9.337
4	49	-9.72	-9.279
ΔNBD2 *147 out of 750 poses in the 4 out of 54 clusters*			
1	11	-9.64	-8.645
2	50	-9.19	-8.165
3	27	-8.89	-8.434
4	59	-8.8	-8.14

[1]The number of poses in a given cluster.
[2]The lowest energy in the given cluster; kcal/mol.
[3]The average energy calculated from the energy of poses in the given cluster; kcal/mol.